JOURNAL OF Applied Polymer SCIENCE

Synthesis of Polyvinylidene Fluoride (PVDF) Membranes for Protein Binding: Effect of Casting Thickness

A. L. Ahmad,[1] N. Ideris,[1] B. S. Ooi,[1] S. C. Low,[1] A. Ismail[2]
[1]School of Chemical Engineering, Engineering Campus, Universiti Sains Malaysia, Seri Ampangan, 14300 Nibong Tebal, S.P.S, Penang, Malaysia
[2]Institute for Research in Molecular Medicine, Health Campus, Universiti Sains Malaysia, 16150 Kubang Kerian, Kelantan, Malaysia
Correspondence to: A. L. Ahmad (E-mail: chlatif@eng.usm.my)

ABSTRACT: Microporous polyvinylidene fluoride (PVDF) membranes were synthesized from PVDF/N-methyl-2-pyrrolidinone (NMP) solutions using an immersion–precipitation method with a 2-propanol/water mixture as a soft coagulant. The effects of membrane thickness on pore size distribution and surface/cross-section morphology were studied using capillary flow porometry and scanning electron microscopy (SEM), respectively. All the synthesized membranes had a small range of pore size distribution, with the pore size decreasing with increasing casting thickness. The semicrystalline PVDF membranes demonstrated significant variations in morphology under SEM observation, with the existence of polymer agglomeration at a casting thickness of 500 μm and above. The protein binding capacity was observed to be highest at a casting thickness of 400 μm, where optimum pore morphology provided a large surface area for protein binding. © 2012 Wiley Periodicals, Inc. J. Appl. Polym. Sci. 128: 3438–3445, 2013

KEYWORDS: synthesis; membranes; morphology

Received 16 January 2012; accepted 26 August 2012; published online 27 September 2012
DOI: 10.1002/app.38522

INTRODUCTION

Membrane-based immunoassays are widely used in a number of scientific and medical fields. An important component of the technique is the transport membrane,[1] which serves as the assay capture matrix.[2] Among the different polymeric materials used as the transport membrane, polyvinylidene fluoride (PVDF) has a lot of potential,[1] due to the high level of nonspecific interaction between the membrane and the protein. In addition, PVDF is a semicrystalline polymer that is well known for being thermally stable, possessing high mechanical strength and low surface energy relative to other polymers, and having excellent resistance to most corrosive chemicals and organic compounds.[3]

Other striking features of PVDF are its high hydrophobicity and its electrostatic properties, which make it useful in biomedical and healthcare devices. However, intrinsic chemical composition is not the only factor affecting the suitability of the membrane for these applications; the morphological properties, too, play a significant role. By selecting the correct membrane polymer type and fabrication parameters, the morphology of the membrane can be varied and could potentially be tailored for specific proteins, making it valuable for different application and analyses. Therefore, a study that focuses on the effect of membrane surface properties and internal layers is important for the development of more effective and accurate immunological analysis techniques.

There have been a number of previous reports on achieving control of the binding between the protein and the membrane by altering the membrane formulation,[4–7] including studies on the effect of polymer concentration, dissolving temperature, solvent, and addition of additives. In addition, modification of the membrane through processes such as crosslinking[8] or reactive gas plasma treatment[9] have been carried out for enhancing protein binding performance. The interaction between the membrane and protein was extensively investigated in these studies, especially with regard to protein purification and recovery. However, to the best of our knowledge, there have been no studies that specifically examine the effect of the thickness of PVDF membrane casting on protein binding performance for immunoblotting applications.

In the present study, membranes were prepared using an immersion–precipitation method, through either a liquid–liquid demixing process and/or crystallization.[10] Based on the

© 2012 Wiley Periodicals, Inc.

CosMX Exhibit 1018, Page 1 of 8

10974628, 2013, 5, Downloaded from https://onlinelibrary.wiley.com/doi/10.1002/app.38522 by University Of Massachusetts Amherst, Wiley Online Library on [27/01/2023]. See the Terms and Conditions (https://onlinelibrary.wiley.com/terms-and-conditions) on Wiley Online Library for rules of use; OA articles are governed by the applicable Creative Commons License

literature, use of a soft coagulation bath can induce crystallization by lowering the liquid–liquid demixing process rate, which subsequently generates a membrane with a symmetrical, microporous structure. This phenomenon can be explained by the Hildebrand solubility parameter difference between the solvent and the coagulation bath. A smaller difference between the parameters for the PVDF and 2-propanol would result in a slow rate of solidification of the nascent membrane, thus creating a membrane with a pore size distribution in the range of microfiltration.

The objective of the current work was to elucidate the effect of membrane morphology on protein binding capacity by investigating casting thickness during membrane fabrication. Evidence shows that initial casting thickness significantly alters membrane properties when phase inversion is involved in the synthesis process. Previous studies have revealed the existence of a critical casting thickness, whereby the morphologies of the fabricated membranes are significantly transformed from a finger-like structure to a sponge-like structure.[11,12] This is an important finding, especially for membrane cross-flow separation. Initial casting thickness has also been demonstrated to influence the formation of macrovoids in the internal structure of polymeric membranes, with an increase in thickness reducing the protein binding performance.[13–15]

However, it is likely that different polymers and fabrication conditions would give different results, and it is well known that many factors contribute to the final morphology of the membrane.[16] Thus, in this study, the formulation and casting conditions were held constant to ensure that the final morphology obtained was a direct effect of the variation in initial casting thickness. The improved understanding of the mechanism of membrane formation acquired in this study can be used in the future development of membranes with enhanced performance for immunoblotting applications.

EXPERIMENTAL

Membrane Preparation

PVDF (Solef 6010/1001, Solvay Solexis) (15 wt %) was dissolved in 85 wt % *N*-methyl-2-pyrrolidinone (NMP) anhydrous (99.5%, Sigma–Aldrich) in a sealed water-jacketed flask under continuous agitation with a stir bar (3.5 cm in length, 500 rpm) for 6 h at 27°C. Before casting, the PVDF solution was sonicated for 1 h at room temperature to remove trapped bubbles.

To form the membrane, the PVDF solution was cast using an automatic film applicator (Elcometer 4340 Motorised, Elcometer, UK). The initial thickness of the membrane was controlled by sliding the desired measuring blade into the gap between the adjustable stroke and the supported glass. In this experiment, the casting thickness was set to 300, 400, 500, 600, and 700 μm. The thickness gauge consisted of blades of different thicknesses ranging from 50 to 800 μm.

The nascent membrane was then immediately immersed in a coagulation bath consisting of a mixture of 2-propanol (99.8%, ACS, ISO, Reag. PhEur, Merck) and deionized water (75 : 25 volume ratio), at room temperature for 24 h. Prior to use, the formed membranes were dried in a humidity chamber at 40°C with a relative humidity of 60% for 3 h. To confirm the reproducibility of membrane synthesis, identical casting formulation and conditions were repeated twice for each casting thickness.

Membrane Characterization

The thermal behavior of the membrane samples was analyzed using differential scanning calorimetry (DSC 6 Perkin Elmer, USA) at a heating rate of 10°C min^{-1}. FTIR (OMNIC FTIR iS10 Nicolet, Thermo Scientific, USA) was used to obtain IR spectra of the prepared PVDF membranes. The α and β forms could be characterized by the absorption peaks at 763 and 840 cm^{-1}, respectively.[17]

Pore size distribution of synthesized membranes was measured using capillary flow porometry (Porolux 1000, Benelux Scientific, Belgium). In this method, each membrane sample was cut into pieces 2 cm in diameter and immersed in perfluorinated wetting liquid (Porefil 12) for ~3 min. The sample analysis was initiated by applying nitrogen gas under increasing pressure with a maximum flow rate of 200 mLmin^{-1}. This method essentially measures the pressure needed to blow inert gas through a liquid-filled membrane, based on the Young–Laplace equation[18]:

$$\Delta P = \frac{2\gamma \cos\theta}{r} \tag{1}$$

where ΔP is the differential gas pressure, γ is the surface tension of wetting liquid (12 dynes cm^{-1}), θ is the wetting angle, and r is the pore radius. The gas pressure is gradually increased with the smallest pores requiring the highest pressure to empty them. At sufficiently high pressure, all the pores become empty and the flow through the wet sample becomes identical to the measured flow through a control dry sample, in which all the pores are empty. In this method, the wetting angle is assumed to be zero. The shape factor used is 0.715, which is based on the assumption that the membrane pores are asymmetric and that they do not have an exact cylindrical shape.[19,20] To confirm the reproducibility of the experimental data, three samples from each membrane were used to determine the values.

The surface and cross-section morphologies of the prepared membranes were observed using scanning electron microscopy (FESEM Carl Zeiss, Supra 35VP, Germany), using a 1000× magnification. For cross-sectional analysis, the membrane was fractured by immersing the sample in liquid nitrogen for ~10 min and then attached to the sample holder using conductive carbon tape. All membrane samples were coated with a Au–Pd alloy to enhance electronic conductivity and then observed with SEM using a 10 kV acceleration voltage with a SE2 detector. The final membrane thickness was measured based on the scale provided by the microscope software using the Java-based image processing program, Image J (1.32j, National Institutes of Health, USA) and further confirmed with a micro thickness gauge (Mitutoyo 7301, Japan). At least, five areas per sample were measured to confirm the reproducibility of the yield thickness.

The membrane porosity, ε, was defined as the pore volume divided by the total volume of the porous membrane. It was

CosMX Exhibit 1018, Page 2 of 8

10974628, 2013, 5, Downloaded from https://onlinelibrary.wiley.com/doi/10.1002/app.38522 by University Of Massachusetts Amherst, Wiley Online Library on [27/01/2023]. See the Terms and Conditions (https://onlinelibrary.wiley.com/terms-and-conditions) on Wiley Online Library for rules of use; OA articles are governed by the applicable Creative Commons License

Applied Polymer SCIENCE

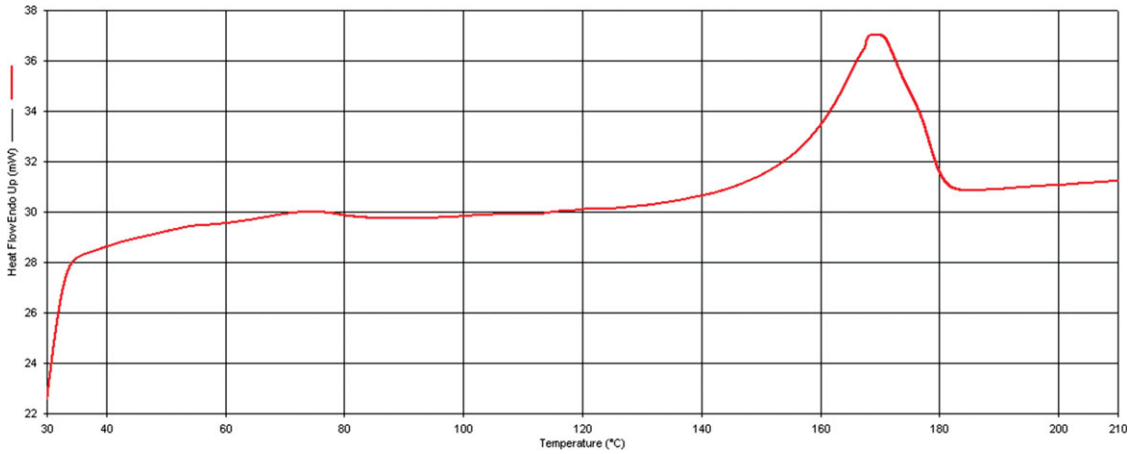

Figure 1. DSC endotherms of PVDF membrane scanned at 10°C min^{-1}. [Color figure can be viewed in the online issue, which is available at wileyonlinelibrary.com.]

determined by weighing the dry sample, soaking it in 2-butanol (≥99.0%, Merck) for 2 h to fill all the pores, drying the surface with filter paper, and then reweighing it. Equation (2) was subsequently used to calculate the values for ε.[21]

$$\varepsilon = \frac{(W_B - W_M)/\rho_B}{(W_B - W_M)/\rho_B + W_M/\rho_P} \times 100\% \qquad (2)$$

where ε is the porosity of the membrane, W_B is the weight of the wet membrane, W_M is the weight of the dry membrane, ρ_B is the specific gravity of 2-butanol (0.81 g cm^{-3}), and $\rho_P$is the specific gravity of PVDF (1.78 g cm^{-3}) (assuming that all materials retained their specific gravity in the wetted membranes and that there was no air trapped in the membrane pores). The 2-butanol was chosen as the wetting liquid as it was able to sufficiently wet the hydrophobic PVDF membrane, and therefore fill all the pores, and because it did not swell the membrane. To confirm the reproducibility of the experimental data, three samples from each membrane were used to determine the ε value.

Protein Binding Capacity

The protein binding capacity was measured for samples with a 12 mm diameter with a known total membrane volume. Each sample was incubated in 3 mL of bovine serum albumin (BSA) solution in 0.05 *M* phosphate buffer (pH 7.0, 3 $mgmL^{-1}$) and shaken at 100 rpm for 3 h at 27°C. Any unbound BSA was removed by washing twice with phosphate buffer with agitation at 100 rpm for 2 min and a volume of 5 mL and then 10 mL. Each membrane sample was then transferred to a test tube to enable quantification of the adsorbed protein using the bicinchoninic acid (BCA) assay. First, 2 mL of BCA working reagent (Merck, Germany) were added, and the test tubes were incubated at 37°C for 30 min. The BSA concentration from the incubated test tube was then calculated by measuring the absorbance of the solution at 562 nm using a spectrophotometer (Spectronic Genesys, USA) and comparing the values to a standard curve of known protein concentrations. At least, five samples from each membrane were used to determine the protein binding to confirm the reproducibility of the experimental data.[5]

RESULTS AND DISCUSSION

PVDF is a hydrophobic semicrystalline polymer with electrostatic properties that make it a valuable material for achieving a high level of protein binding. Prior to studying the effects of casting thickness on membrane morphology, the physicochemical properties of the PVDF membrane were examined to verify the crystalline structure. DSC tests demonstrated the presence of the predicted crystallinity with thermal behavior in accordance with the literature and a similar melting temperature of ~170°C (Figure 1).[3]

Following this, the crystalline phases were further confirmed using FTIR analysis. Peaks at 763 and 840 cm^{-1}, corresponding to the α and β phase, respectively, can be seen in the spectra shown in Figure 2.[17] In addition, the peak due to the β phase is slightly higher than that of the α phase, indicating that the β phase is dominant for this particular membrane material. Under the correct physicochemical conditions, a higher proportion of β phase is preferable as it should help to improve the membrane protein binding interaction.

To investigate the effect of casting thickness on membrane morphology, solutions of PVDF of the same concentration were cast at room temperature to obtain thicknesses in the range of 300–700 μm. The pore size distribution for each membrane was measured using capillary flow porometry, and the pores throughout the entire polymer matrix of the membrane, not just the surface, were taken into consideration. The pressure applied is inversely proportional to the pore radius [eq. (1)], so the smaller the pore size, the higher pressure is required. If a high proportion of pores were of a similar size then there would be a peak in the measured nitrogen flow at a specific corresponding applied pressure. In this method, only through-pores were analyzed, which are those that are open to both sides of the membrane; therefore, the effectiveness of the membrane could be determined.

CosMX Exhibit 1018, Page 3 of 8

10974628, 2013, 5, Downloaded from https://onlinelibrary.wiley.com/doi/10.1002/app.38522 by University Of Massachusetts Amherst, Wiley Online Library on [27/01/2023]. See the Terms and Conditions (https://onlinelibrary.wiley.com/terms-and-conditions) on Wiley Online Library for rules of use; OA articles are governed by the applicable Creative Commons License

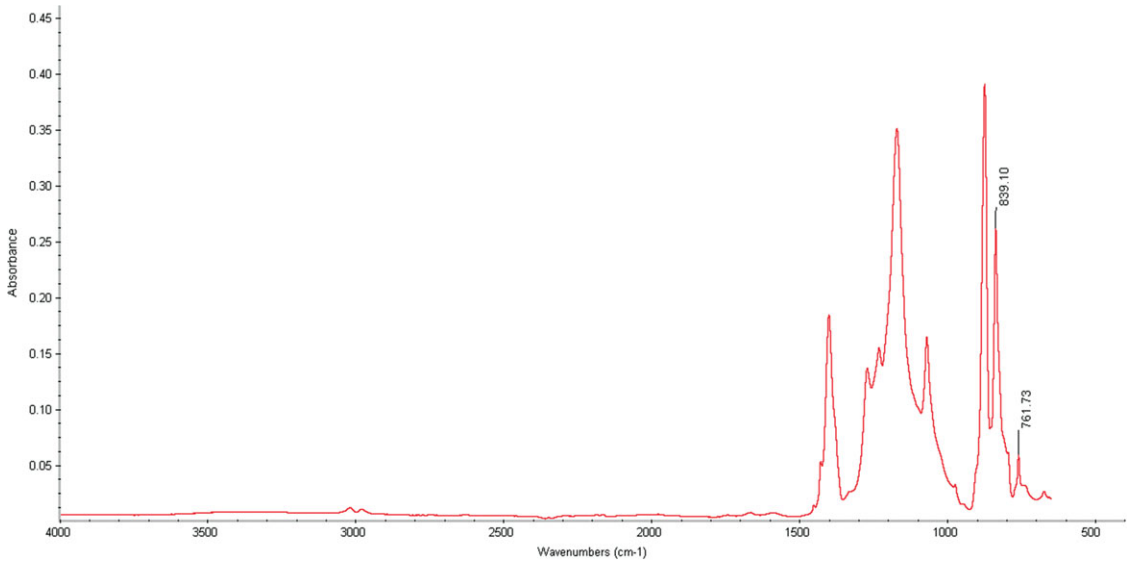

Figure 2. FTIR spectra of PVDF membranes. [Color figure can be viewed in the online issue, which is available at wileyonlinelibrary.com.]

The gas flows through the wet and dry samples were then used to calculate the pore size distribution based on the relative flow rate, RF (%), which was determined using eq. (3).[22]

$$\text{Relative Flowrate, RF}\,(\%) = \frac{\text{wet flow}}{\text{dry flow}} \times 100\% \qquad (3)$$

The RF values were then inserted into eq. (4) to determine the values for relative pore size distribution of each membrane sample.[22] The leading negative sign is present because a decrease in pore size causes an increase in pressure [eq. (1)], and thus, an increase in flow rate.

$$\text{Relative pore size distribution} = \frac{\text{Current RF}\,(\%) - \text{Previous RF}\,(\%)}{-\,(\text{Current diameter} - \text{Previous diameter})} \qquad (4)$$

Figure 3 shows the wet and dry curves obtained for the membrane samples. It can be seen that for samples cast at 400–700 μm, the wet and dry curves eventually reached a stable pressure, which indicated that the samples were fully analyzed and the smallest pores had been included in the measurements. However, for membranes with a casting thickness of 300 μm, the wet and dry curves only met at the end of the analysis period, and ran in parallel from a starting pressure of ~0.8 bar. It was concluded that the wetting liquid had not been fully purged from the sample due to the presence of closed pores. These may be due to the fact that through-pores cannot be formed completely when the membrane has this particular thickness.

Because the increase in the percentage flow is essentially determined by the increase in the number of pores at a specific pore diameter, a sharp rise in flow distribution suggests the number of pores of that diameter is large. It can be seen from Figure 3 that at ~0.8 bar, a sharp increase in flow rate occurred for the sample of 300 μm casting thickness. As the casting thickness increased, the pressure required for this jump in flow rate increased. Thus, based on eq. (1), it was deduced that a higher casting thickness resulted in smaller pore sizes. The values of

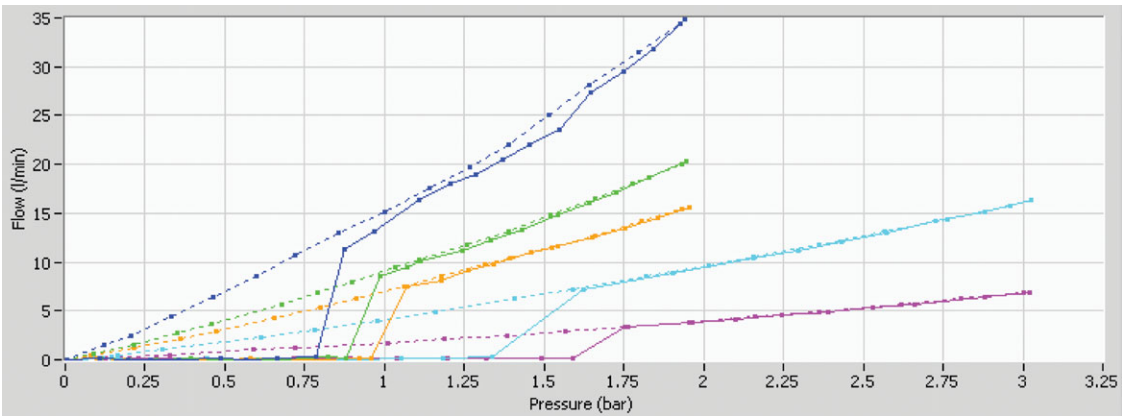

Figure 3. Wet and dry porometry curves for membranes of different casting thicknesses: 300 μm (left), followed by 400, 500, 600, and 700 μm (right). [Color figure can be viewed in the online issue, which is available at wileyonlinelibrary.com.]

CosMX Exhibit 1018, Page 4 of 8

10974628, 2013, 5, Downloaded from https://onlinelibrary.wiley.com/doi/10.1002/app.38522 by University Of Massachusetts Amherst, Wiley Online Library on [27/01/2023]. See the Terms and Conditions (https://onlinelibrary.wiley.com/terms-and-conditions) on Wiley Online Library for rules of use; OA articles are governed by the applicable Creative Commons License

Applied Polymer SCIENCE

Table I. Smallest Pore Size, Bubble Point Pore Size, and Mean Pore Size

Initial casting thickness (μm)	Smallest pore size (μm)	Bubble point pore size (μm)	Mean pore size (μm)
300	0.3911 ± 0.0295	0.4433 ± 0.0066	0.4188 ± 0.0085
400	0.1909 ± 0.0333	0.3957 ± 0.0094	0.3742 ± 0.0041
500	0.1463 ± 0.0067	0.3613 ± 0.0315	0.3373 ± 0.0198
600	0.1363 ± 0.0090	0.2689 ± 0.0236	0.2456 ± 0.0102
700	0.1330 ± 0.0288	0.2360 ± 0.0398	0.1883 ± 0.0008

the smallest pore sizes and the bubble-point pore size (corresponding to biggest pore size) are listed in Table I. This shows that all values are in line with the increasing pressure.

Figure 4 shows the values of RF [Figure 4(a)] and pore size distribution [Figure 4(b)] for all membrane samples. For the RF, it can be seen that all the membrane samples reached 100%, indicating that the gas flow rate of wet and dry samples was equal at a specific pressure. It was also observed that the slopes of the curves for all samples were steep, corresponding to a narrow pore size distribution. For membranes with a casting thickness of 300 μm, the pore size distribution was in the range of 0.35–0.44 μm [Figure 4(b)]. As the membrane thickness increased, the pore size distribution gradually decreased to ~0.32–0.39 μm, 0.28–0.36 μm, 0.18–0.26 μm, and 0.18–0.22 μm, for thicknesses of 400, 500, 600, and 700 μm, respectively. The mean pore sizes of the membranes are listed in Table I, reflecting the pore size that is dominant for each casting thickness. The demonstrated pore size distribution is due to a lower diffusion rate of nonsolvent in the thicker cast films. This leads to a delay in liquid–liquid phase demixing. Therefore, the membrane pore size was shifted to lower values as the casting thickness increased.[23] The peaks for all the membrane samples appeared sharp, indicating that most of the pore diameters were close to the mean pore diameter. These results were further supported by the SEM micrographs of the membrane surfaces presented in Figure 5(a–e).

The SEM images were then used to determine the cross sections of the membranes. Figure 5 shows the cross-section morphologies of the PVDF membranes, fabricated at different casting thicknesses (300–700 μm). It can be clearly seen from the

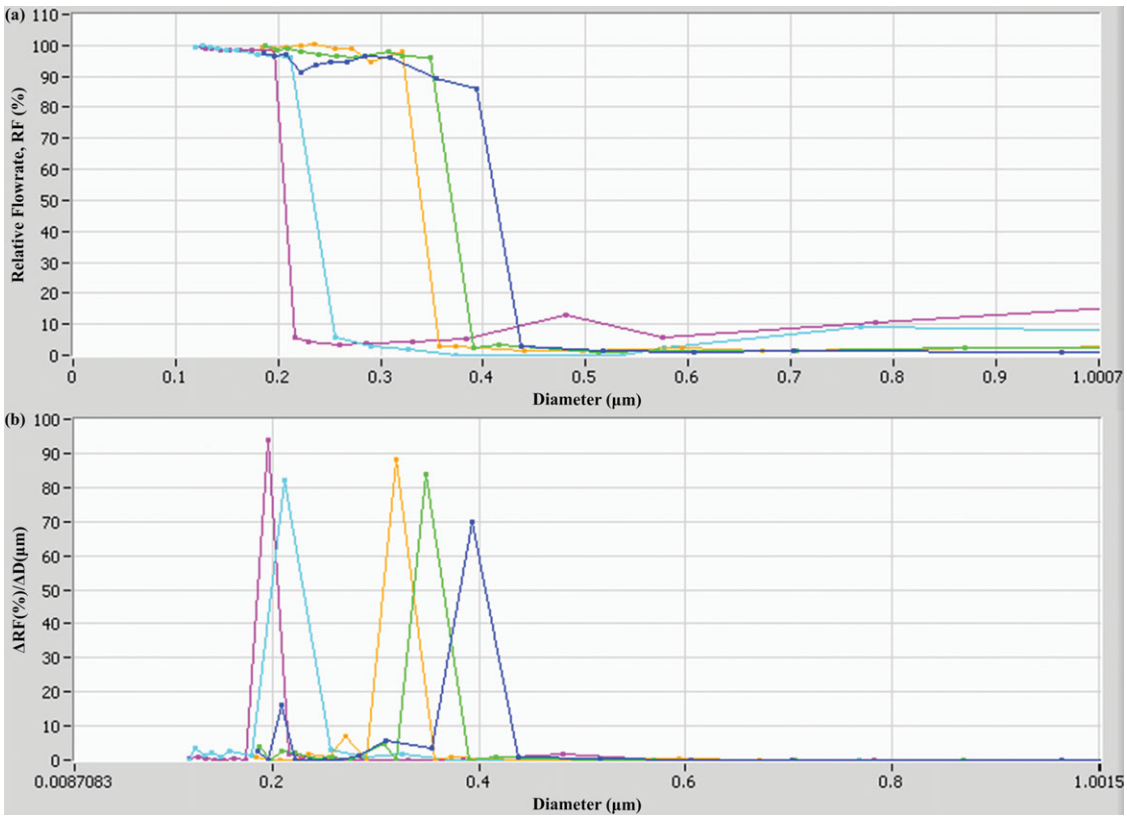

Figure 4. (a) Relative flow rate (%) and (b) Pore size distribution for membranes of different casting thicknesses: 700 μm (left), followed by 600, 500, 400, and 300 μm (right). [Color figure can be viewed in the online issue, which is available at wileyonlinelibrary.com.]

CosMX Exhibit 1018, Page 5 of 8

10974628, 2013, 5, Downloaded from https://onlinelibrary.wiley.com/doi/10.1002/app.38522 by University Of Massachusetts Amherst, Wiley Online Library on [27/01/2023]. See the Terms and Conditions (https://onlinelibrary.wiley.com/terms-and-conditions) on Wiley Online Library for rules of use; OA articles are governed by the applicable Creative Commons License

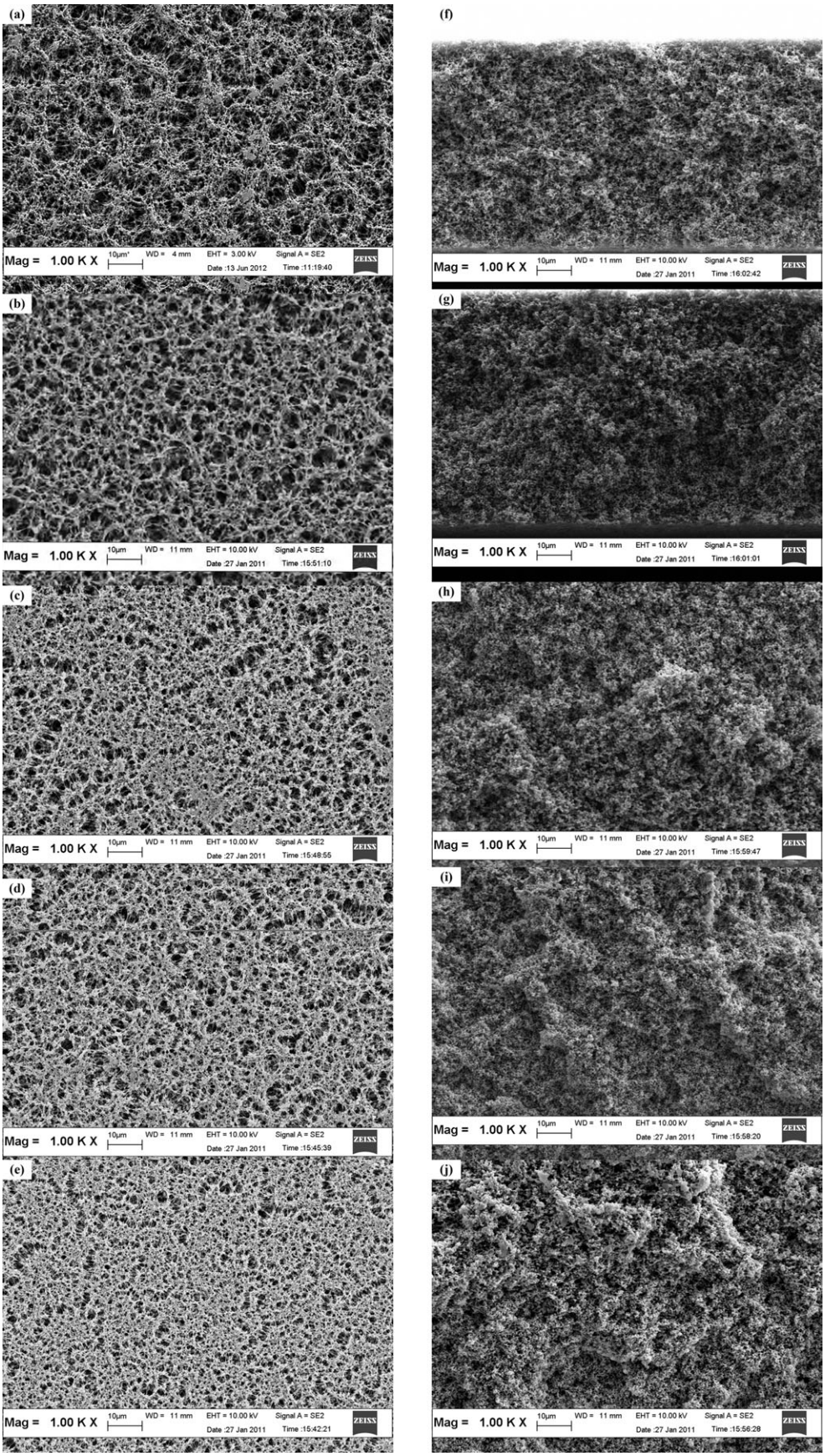

Figure 5. Effect of casting thickness on membrane surface and cross-section morphologies. Dope solutions of 15 wt % PVDF in NMP were cast at different casting thickness: (a, f) 300 μm, (b, g) 400 μm, (c, h) 500 μm, (d, i) 600 μm, and (e, j) 700 μm.

CosMX Exhibit 1018, Page 6 of 8

10974628, 2013, 5, Downloaded from https://onlinelibrary.wiley.com/doi/10.1002/app.38522 by University Of Massachusetts Amherst, Wiley Online Library on [27/01/2023]. See the Terms and Conditions (https://onlinelibrary.wiley.com/terms-and-conditions) on Wiley Online Library for rules of use; OA articles are governed by the applicable Creative Commons License

Applied Polymer SCIENCE

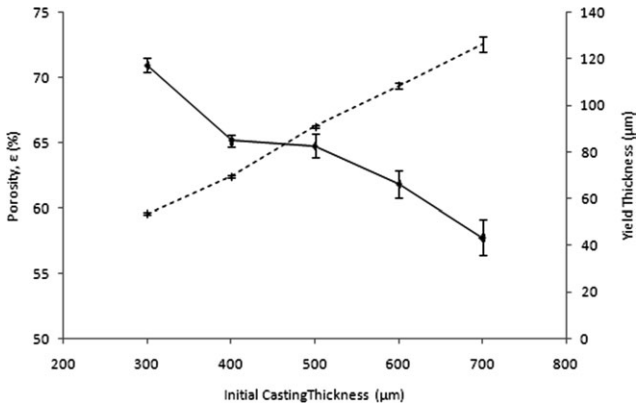

Figure 6. Porosity values (%) and yield thickness of the PVDF membranes prepared with different casting thicknesses.

images [Figure 5(f–j)], that a symmetrical membrane was obtained for all membrane samples. The cross-sectional structure did not vary along the entire thickness, and there was no evidence of macrovoid formation.[16] A porous structure was observed in the cross-sectional images of the membranes with thicknesses of 300 and 400 μm [Figure 5(f, g)], with no appearance of polymer agglomeration. However, with increasing thickness, the membrane cross-section structure became more compact and dense. Polymer agglomeration is evident in the images of 500 μm membranes and becomes clearer with further increases in thickness.

For porous membranes synthesized from semicrystalline polymers, such as PVDF, the immersion precipitation process is governed primarily by two types of phase separation: crystallization and liquid–liquid demixing. Usually, the use of a soft coagulation bath will induce a crystallization process to commence much earlier than liquid–liquid demixing, due to slow mass exchange. This slow mass exchange contributes directly to the lower solubility parameter difference between the solvent and nonsolvent. In this experiment, the solubility parameter of the mixture used as a soft coagulant is ~29.6 MPa,$^{1/2}$ which is relatively close to the solvent's solubility parameter (22.9 MPa$^{1/2}$), in contrast with other common coagulation baths such as water (47.9 MPa$^{1/2}$).[24] Because the membrane dope solution was prepared under exactly the same conditions, it is expected that the nascent membranes were under similar thermodynamic conditions. Therefore, the final membrane morphology was mostly determined by the kinetics of the phase inversion process.

In this study, the formed membranes were directly immersed in the soft coagulation bath mixture of 2-propanol and water. The process of phase inversion would start to occur on the upper part of the membrane, as it is the most exposed layer; the membranes would then solidify slowly. The existence of the solid layer on the upper part of the membrane will create more resistance for the occurrence of a liquid–liquid demixing process. The speed of polymer matrix formation will be much slower in the central and lower parts as more layers are involved in the membrane formation. If the process of liquid–liquid demixing is too slow, it will allow more time for the polymer nuclei to crystallize. Excessive crystal growth will induce polymer agglomeration, as can be seen in Figure 5. This slow process will also cause the membrane structure to become denser in a thicker membrane.

These SEM cross-section results were further corroborated by the porosity tests. Figure 6 shows that increasing casting thickness caused the membrane porosity to decrease significantly from 70.97% ± 0.57% to 57.77% ± 1.35%. As previously discussed, a higher casting thickness caused the exchanging process between the solvent and the nonsolvent to become much slower, and thus, the membrane structure became denser and more compact, subsequently leading to lower porosity for the thicker membranes. Figure 6 also shows the final yield thickness of the synthesized membranes. As expected, the yield thickness is in line with the initial casting thickness, with only small errors being observed for each membrane sample.

Structural properties such as pore radius, pore volume (porosity), and cocontinuity of pores affect the internal surface area of the membrane, which is of great importance when using the membranes in biomedical applications. Thus, the performance of the fabricated membrane was tested in terms of protein binding capability, whereby higher protein retention is desired. As stated in the literature, the most important driving forces for protein binding are electrostatic and hydrophobic interactions.[25] The electrostatic effects are observed when the charges between the protein and the membrane surface are opposite, which, however, might be influenced by dilution or changing the pH. However, on a hydrophobic surface such as that of the PVDF membrane, the hydrophobic interaction dominates, allowing for high protein binding, even under electrostatically adverse conditions.[26]

Figure 7 shows clearly that protein binding increased from 6275.66 ± 120.56 μg cm^{-3} to 6761.10 ± 52.75 μg cm^{-3} at casting thicknesses of 300 and 400 μm, respectively. However, as the membrane thickness increased from 400 to 700 μm, the protein binding performance of membrane dropped from 6761.10 ± 52.75 μg cm^{-3} to 5831.46 ± 285.01 μg cm^{-3}. These results correlate with the variations in the morphology of the microporous membranes. In general, a combination of smaller pore size and higher porosity is required for obtaining microporous membranes with a high degree of interconnection between the

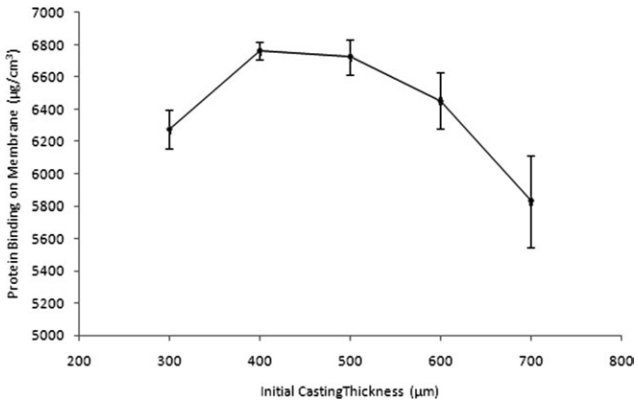

Figure 7. Effect of initial casting thickness on protein binding performance.

CosMX Exhibit 1018, Page 7 of 8

10974628, 2013, 5, Downloaded from https://onlinelibrary.wiley.com/doi/10.1002/app.38522 by University Of Massachusetts Amherst, Wiley Online Library on [27/01/2023]. See the Terms and Conditions (https://onlinelibrary.wiley.com/terms-and-conditions) on Wiley Online Library for rules of use; OA articles are governed by the applicable Creative Commons License

pores.[27] This morphology is desired as it maximizes the internal surface area for hydrophobic and electrostatic interactions between membrane and protein. Among all the samples, membrane with initial casting thickness of 400 μm showed the lowest standard error ($\pm$ 52.75), with the highest error observed for a thickness of 700 μm ($\pm$ 285.01). This result is due to the better homogeneity of the membrane with a casting thickness of 400 μm, as supported by the pore size distribution data and SEM images.

Membranes cast with a thickness of 300 μm provided the highest porosity, with a percentage value of 70.97%. However, the results from the capillary flow porometry show that a through-pore structure was not thoroughly formed, thus creating a morphology that was not effective in capturing protein. At a casting thickness of 700 μm, the protein binding performance was the lowest, with only 5831.46 μg cm^{-3} being retained. Therefore, even though a smaller pore size is desired, the pore volume (porosity) of the membrane sample must also be considered. It was discussed previously that the 700 μm membrane showed some polymer agglomeration that caused the structure to become denser, and as a result, the capturing area for protein decreased. Based on Figure 7, it is clear that the highest protein binding performance recorded was achieved at a casting thickness of 400 μm with retention of 6761.10 $\pm$ 52.75μg cm^{-3} of BSA.

CONCLUSION

Microporous PVDF membranes were prepared using an immersion–precipitation method at different casting thicknesses. The formed membranes all exhibited different membrane morphologies with both pore size distribution and porosity decreasing with increasing membrane thickness. A membrane casting thickness of 400 μm was seen to provide the best balance between pore size distribution and porosity, and therefore, a large internal surface area for protein binding. The thickness of 400 μm was therefore considered to be the best among the five different casting thicknesses.

ACKNOWLEDGMENTS

The authors acknowledge Universiti Sains Malaysia, USM (Vice-Chancellor Award 2010), USM-PGRS Grant (8034059), USM Membrane Cluster (8610012), and ERGS Grant (6730004) for financial support.

REFERENCES

1. Aizawa, K.; Gantt, E. *Anal. Chim. Acta* **1998,** *365*, 109.
2. Mistrello, G.; Gentili, M.; Falagiani, P.; Roncarolo, D.; Riva, G.; Tinelli, M. *Immunol. Lett.* **1995,** *47*, 79.
3. Ebnesajjad, S. Fluoroplastics: Non-Melt Processible Fluoroplastics. The Definitive User's Guide and Databook; Plastics Design Library: New York, **2000;** Vol. *1*.
4. Wang, T.; Wang, Y.-Q.; Su, Y.-L.; Jiang, Z.-Y. *Colloids. Surf. B Biointerfac.* **2005,** *46*, 233.
5. Ahmad, A. L.; Low, S. C.; Shukor, S. R. A.; Ismail, A. *J. Appl. Polym. Sci.* **2008,** *108*, 2550.
6. Tanyolaç, D.; SönmezIsIk, H.; Özdural, A. R. *Biochem. Eng. J.* **2005,** *22*, 221.
7. Mockel, D.; Staude, E.; Guiver, M. D. *J. Membr. Sci.* **1999,** *158*, 63.
8. Zhao, Z.-P.; Wang, Z.; Wang, S.-C. *J. Membr. Sci.* **2003,** *217*, 151.
9. Greene, G.; Radhakrishna, H.; Tannenbaum, R. *Biomaterials* **2005,** *26*, 5972.
10. Buonomenna, M. G.; Macchi, P.; Davoli, M.; Drioli, E. *Eur. Polym. J.* **2007,** *43*, 1557.
11. Li, D.; Chung, T.-S.; Ren, J.; Wang, R. *Ind. Eng. Chem. Res.* **2004,** *43*, 1553.
12. Azari, S.; Karimi, M.; Kish, M. H. *Ind. Eng. Chem. Res.* **2010,** *49*, 2442.
13. Vogrin, N.; Stropnik, C.; Musil, V.; Brumen, M. *J. Membr. Sci.* **2002,** *207*, 139.
14. Conesa, A.; Gumí, T.; Palet, C. *J. Membr. Sci.* **2007,** *287*, 29.
15. Ahmad, A. L.; Low, S. C.; Shukor, S. R. A. *Script. Mater.* **2007,** *57*, 743.
16. Mulder, M. Basic Principles of Membrane Technology; Kluwer Academic Publishers: Netherlands, **1996.**
17. Salimi, A.; Yousefi, A. A. *Polym. Test.* **2003,** *22*, 699.
18. Kaur, S.; Ma, Z.; Gopal, R.; Singh, G.; Ramakrishna, S.; Matsuura, T. *Langmuir* **2007,** *23*, 13085.
19. Operating Manual IBFT Porometer, Beneflux Scientific. in V1.08EN, Eke Belgium, **2010**.
20. Lowell, S.; Martin, J. E. S.; Thomas, A.; Thommes, M. Characterization of Porous Solids and Powders: Surface Area, Pore Size and Density; Springer: Dordrecht, **2006.**
21. Nguyen, Q. T.; Alaoui, O. T.; Yang, H.; Mbareck, C. *J. Membr. Sci.* **2010,** *358*, 13.
22. Low, S. C.; Ahmad, A. L.; Ideris, N.; Ng, Q. H. Bioresour. *Technol.* **2011,** *113*, 219.
23. Zhang, S.; Wang, K. Y.; Chung, T.-S.; Jean, Y. C.; Chen, H. *Chem. Eng. Sci.* **2011,** *66*, 2008.
24. Burke, J. Solubility Parameters: Theory and Application; The Oakland Museum of California, **1984**; Available at: http://books.google.com.my/books?id=DQvzcQAACAAJ; http://cool.conversation-us.org/coolaic/sg/bpg/annual/v03/bpo3-04.html.
25. Giacomelli, C. E. In Encyclopedia of Surface and Colloid Science; Hubbart, A. T., Ed.; Taylor & Francis: Boca Raton, FL, **2006,** 510.
26. Norde, W. Driving Forces for Protein Adsorption at Solid Surfaces; M. Dekker: New York, **1998.**
27. Baker, R. W. In Encyclopedia of Polymer Science and Technology; Mark, H. F., Ed.; Wiley: New Jersey, **2003;** p 184.

CosMX Exhibit 1018, Page 8 of 8

10974628, 2013, 5, Downloaded from https://onlinelibrary.wiley.com/doi/10.1002/app.38522 by University Of Massachusetts Amherst, Wiley Online Library on [27/01/2023]. See the Terms and Conditions (https://onlinelibrary.wiley.com/terms-and-conditions) on Wiley Online Library for rules of use; OA articles are governed by the applicable Creative Commons License